⌘ *Author's Choice*

THE JOURNAL OF BIOLOGICAL CHEMISTRY VOL. 284, NO. 42, pp. 28674–28681, October 16, 2009


# The Three-dimensional Structure of Carnocyclin A Reveals That Many Circular Bacteriocins Share a Common Structural Motif*[S]

Received for publication, June 23, 2009, and in revised form, August 4, 2009 Published, JBC Papers in Press, August 18, 2009, DOI 10.1074/jbc.M109.036459

**Leah A. Martin-Visscher[‡], Xiandi Gong[§], Marek Duszyk[§], and John C. Vederas[‡1]**

*From the Departments of [‡]Chemistry and [§]Physiology, University of Alberta, Edmonton, Alberta T6G 2G2, Canada*

**Carnocyclin A (CclA) is a potent antimicrobial peptide from *Carnobacterium maltaromaticum* UAL307 that displays a broad spectrum of activity against numerous Gram-positive organisms. An amide bond links the N and C termini of this bacteriocin, imparting stability and structural integrity to this 60-amino acid peptide. CclA interacts with lipid bilayers in a voltage-dependent manner and forms anion selective pores. Several other circular bacteriocins have been reported, yet only one (enterocin AS-48) has been structurally characterized. We have now determined the solution structure of CclA by NMR and further examined its anion binding and membrane channel properties. The results reveal that CclA preferentially binds halide anions and has a structure that is surprisingly similar to that of AS-48 despite low sequence identity, different oligomeric state, and disparate function. CclA folds into a compact globular bundle, comprised of four helices surrounding a hydrophobic core. NMR studies show two fluoride ion binding modes for CclA. Our findings suggest that although other circular bacteriocins are likely to have diverse mechanisms of action, many may have a common structural motif. This shared three-dimensional arrangement resembles the fold of mammalian saposins, peptides that either directly lyse membranes or serve as activators of lipid-degrading enzymes.**

Bacteriocins are a diverse group of ribosomally synthesized, antimicrobial peptides produced by bacteria. Those made by Gram-positive bacteria are usually cationic and typically have 30–70 residues (1–3). These peptides are substantially more active than conventional antibiotics against numerous pathogenic and drug resistant bacteria, including virulent strains of *Staphylococci*, *Enterococci*, *Listeria*, and *Clostridia*, but they display virtually no toxicity toward eukaryotic cells. The circular bacteriocins are a unique group, characterized by an amide bond linking the N and C termini of the peptide. They exhibit enhanced stability to pH and temperature variation and are resistant to numerous proteases, in contrast to many linear bacteriocins. This stability derives, in part, from the cyclic structure of the peptide (4). Interestingly, circular peptides are not unique to bacteria; they have also been discovered in plants and animals and exhibit a diverse range of bioactivities. Typically, the circular peptides from these higher organisms are shorter in length and contain at least one disulfide bond, further bracing the structure and enhancing stability (5, 6).

We recently isolated carnocyclin A (CclA)[2] from *Carnobacterium maltaromaticum* UAL307 and employed tandem mass spectrometry amino acid sequencing and genetic analysis to confirm that it is a circular bacteriocin (7). This 60-residue peptide displays a broad antimicrobial spectrum and is particularly potent against the serious food pathogen *Listeria monocytogenes.* The producer strain has recently been approved in the United States as an additive for preservation of processed meat products.

Eight other circular bacteriocins have been reported. These include enterocin AS-48 (8), butyrivbriocin AR10 (9), circularin A (10), gassericin A and reutericin 6 (11, 12), subtilosin A (13, 14), uberloysin (15), and most recently, lactocyclicin Q (16). Gassericin A and reutericin 6 have identical primary sequences but differ by the presence of one D-alanine, resulting in different spectra of activity and secondary structure profiles (11). Acidocin B is considered a putative circular protein, as it shows 98% sequence identity to gassericin A and reutericin 6, but its circular nature has not been confirmed (17). Of these bacteriocins, subtilosin A is atypical; it is significantly shorter (35 amino acids), anionic, and contains unique thioether bridges linking cysteine sulfurs to the $\alpha$-carbon of other residues (13, 18, 19). As such, subtilosin A represents a unique class of bacteriocins (13) and will not be included in the present discussion of the other circular bacteriocins. These range from 58–70 amino acids in length, are cationic, and contain a large number of hydrophobic residues (4).

* This work was supported by the Natural Sciences and Engineering Research Council of Canada, the Advanced Foods and Materials Network, and the Canada Research Chair in Bioorganic and Medicinal Chemistry.

⌘ *Author's Choice*—Final version full access.

[S] The on-line version of this article (available at http://www.jbc.org) contains supplemental "Experimental Procedures and Results," "Acknowledgments," references, and Figs. 1–8.

*The atomic coordinates and structure factors (code 2KJF) have been deposited in the Protein Data Bank, Research Collaboratory for Structural Bioinformatics, Rutgers University, New Brunswick, NJ (http://www.rcsb.org/).*

*Chemical shift data for CclA have been deposited in the BioMagResBank, Department of Biochemistry, University of Wisconsin, Madison, WI under accession number 16319.*

[1] To whom correspondence should be addressed: Dept. of Chemistry, University of Alberta, Edmonton, Alberta T6G 2G2, Canada. Tel.: 780-492-5474; Fax: 780-492-2134; E-mail: john.vederas@ualberta.ca.

[2] The abbreviations used are: CclA, carnocyclin A; $\alpha$, $\alpha$-helix; MES, 2-(*N*-morpholine)ethanesulfonic acid; AS-48, enterocin AS-48; NOE, nuclear Overhauser enhancement; HPLC, high performance liquid chromatography; TAPS, [(2-hydroxy-1,1-bis[hydroxymethyl]ethyl)amino]-1-propanesulfonic acid; r.m.s.d., root mean square deviation; HSQC, heteronuclear single quantum coherence; TOCSY, total correlation spectroscopy; COSY, correlation spectroscopy; NOESY, NOE spectroscopy.

To date, the structure of only one of these circular bacteriocins has been in reported. In 2000, González *et al.* (20) described the NMR solution structure of AS-48, revealing that it consists of five helices encompassing a compact hydrophobic core. The covalent bond linking the N and C termini of the peptide was found to reside within the fifth helix. In 2003, crystallographic studies supported the proposal that at physiological pH, AS-48 exists as a water soluble dimer, in which the hydrophobic faces of the individual monomers are in contact and polar interactions with the aqueous solvent are maximized (21). However, upon interaction with a membrane, this dimer undergoes a conformational change, exposing its hydrophobic faces and facilitating insertion into the membrane. The three-dimensional structure of AS-48 shows a significant charge separation across the molecule, as a cluster of lysines at one end of the molecule imparts a high degree of positive charge on the surface of the peptide. This charge localization is believed to be crucial for insertion of the peptide into the membrane through a mechanism known as molecular electroporation (20, 22, 23). Functional studies of AS-48 have shown that this peptide causes nonselective pore formation in lipid bilayers, thereby allowing for the free diffusion of ions and low molecular weight solutes across the membrane (24). A similar mode of action has been reported for gassericin A and reutericin 6 (11).

We have now determined the three-dimensional solution structure of CclA by NMR. Our results reveal that CclA assumes a globular structure, consisting of four helices surrounding a compact, hydrophobic core. The global architecture of CclA and its surface features are remarkably similar to those of AS-48, suggesting a common structural motif for circular bacteriocins that closely resembles the saposin fold, a conserved structural moiety found within the saposin and saposin-like polypeptide families (25, 26). Functional studies show that CclA forms anion selective channels in lipid bilayers (27). We have further characterized these ion channels by examining the anion selectivity of the pores and the effect of pH on channel conductance. NMR studies demonstrate that CclA binds fluoride in two different ways. The results show that despite the shared structural motif of a sapsosin fold, circular bacteriocins can have unique functional properties.

## EXPERIMENTAL PROCEDURES

*Expression and Purification of CclA and {$^{15}$N,$^{13}$C}-CclA*—CclA was purified from *C. maltaromaticum* UAL307 as previously described (7). For NMR studies, CclA was prepared as a doubly labeled {$^{15}$N,$^{13}$C} sample by growing the producer organism in isotopically enriched Celtone CN Complete Media (Cambridge Isotope Laboratories, Inc., Andover, MA). Purification of {$^{15}$N,$^{13}$C}-CclA was identical to that of the unlabeled bacteriocin.

*NMR Spectroscopy of CclA*—{$^{15}$N,$^{13}$C}-CclA was dissolved in 20 mM sodium phosphate (pH 5.9) in 90% $H_2O$ and 10% $D_2O$ to a final concentration of ~1 mM. To prevent sample degradation, 1 mM EDTA, 1 mM $NaN_3$, and protease inhibitors (Roche Applied Science, Laval PQ) were added. 100 $\mu$M 2,2-dimethyl-2-silapentanesulfonic acid was added for referencing. NMR spectra were acquired on a Varian Inova 600 MHz spectrometer, equipped with an HCN probe and *z* axis pulsed field gradients. For backbone chemical shift assignments, the following experiments were performed: 2D-{$^{1}$H–$^{15}$N}-HSQC, 3D-{$^{1}$H–$^{15}$N}-TOCSY-HSQC, 3D-HNCO, 3D-CBCA(CO)NH, 3D-HNCACB. For side chain assignments, the sample was lyophilized and dissolved in an equivalent volume of 100% $D_2O$, and the following experiments were performed: 3D-HCCH-TOCSY, 2D-{$^{1}$H–$^{13}$C}-HSQC (full and aliphatic), 2D-TOCSY and 2D-COSY. Structural restraints were obtained from the following experiments: 3D-{$^{1}$H–$^{15}$N}-NOESY-HSQC, 3D-{$^{1}$H–$^{13}$C}-NOESY-HSQC, 2D-NOESY and 3D-HNHA. Data were processed with NMRPipe (28) and analyzed with NMRView (29).

*Structure Calculations*—The structure of CclA was calculated with CYANA 2.1 (30), using nuclear Overhauser effect (NOE) restraints obtained from the $^{15}$N- and $^{13}$C-edited HSQC-NOESY and 2D-NOESY experiments and angle restraints derived from analysis of the HNHA experiment and from TALOS (31). A combination of manually and automatically assigned NOEs were used and calibrated within CYANA according to their intensities. After seven rounds of calculation (10,000 steps per round), a total of 657 NOE restraints, 43 $^{3}J_{\mathrm{HNH}\alpha}$ coupling constants, and 98 dihedral angle restraints were used in the final calculation. The 20 lowest energy conformations, with no NOE violations of >0.3 Å and no residues in the disallowed region of the Ramachandran plot, were chosen as representative of the solution structure of CclA. Coordinates for CclA have been deposited in the Protein Data Bank (code 2KJF), and chemical shift assignments have been deposited in the BioMagResBank (code 16319). Electrostatic surface calculations were computed with APBS (32), and figures were generated using PyMOL.

*Secondary Structure Analysis and Homology Modeling*—The secondary structure of the circular bacteriocins was predicted with both the Jpred3 (33) and PSIPRED (34, 35) protein structure prediction servers. To allow for the possibility of secondary structure across the N and C termini, each sequence was submitted twice, as follows. In the first instance, the regular linear sequence was submitted, and coil regions were identified from the output. The sequence was then swapped so that a coil region would become the new N terminus, and the former N-terminal residues were added to the C terminus of the sequence. This modified sequence was then submitted for analysis. For homology modeling, the sequences of AS-48, CclA, circularin A, uberolysin, and lactocyclicin Q were aligned with ClustalW (36). The sequences were imported into DeepView Swiss-Pdb viewer (37) and were fitted onto the structure of either AS-48 (Protein Data Bank code 1E68) or CclA, according to the ClustalW alignment. The models were then submitted to the Swiss-Model server for further refinement (37).

*Functional Studies of CclA Ion Channels*—Lipid bilayers and CclA liposomes were prepared as described previously (27). CclA liposomes were added to the bilayer, and single channel recording was carried out as previously described. For anion permeability studies, single channel recording experiments were performed under asymmetric ionic conditions. The *cis* chamber contained 0.5 M NaCl, and the *trans* chamber contained 0.5 M Na*X*, where *X* was $F^-$, $Br^-$, $NO_3^-$, $CH_3COO^-$, or $H_2PO_4^-$. Both chambers were buffered with 10 mM HEPES

(pH 7.4). For pH experiments, the buffer solution was changed from HEPES (for pH 7.4) to either MES for pH 5.0 or to TAPS for pH 9.0. For symmetric pH studies, the same buffer solution was used in both the *cis* and *trans* chambers, whereas for asymmetric studies, the *cis* chamber contained the lower pH solution.

*Fluorine NMR Studies*—CclA was dissolved in 90% $H_2O$ and 10% $D_2O$ water to a concentration of 1 mM. The pH of the sample was 3.8, due to residual trifluoroacetic acid following HPLC purification. The sample was titrated with sodium fluoride (adjusted to pH 3.8) by addition of 0.5, 1, 1.5, 2, and 3 molar eqs of sodium fluoride. The resulting one-dimensional fluorine spectra were monitored by NMR on a Varian VNMRS 500 MHz spectrometer equipped with a $^{1}H$ $^{19}F$ Z gradient probe capable of $^{19}F$ direct detection. Control experiments with sodium fluoride and trifluoroacetic acid in the absence of protein were also performed at pH 3.8.

## RESULTS AND DISCUSSION

*Preliminary Structural Studies*—Prior to initiating NMR studies, a stereochemical analysis of the constituent amino acids in CclA was done, as two of the circular bacteriocins (gassericin A and reutericin 6) are known to contain D-residues (11). Following hydrolysis, derivatization, and chiral gas chromatography mass spectrometry, it was found that that CclA contains only L-amino acids (supplemental Fig. 1). Complete experimental details are listed in the supplemental data. To determine the oligomeric state of CclA under different pH and salt conditions, a combination of dynamic light scattering and NMR experiments were performed. Our results show that, in contrast to AS-48, CclA is monomeric under physiological conditions (details listed in supplemental data).

*Chemical Shift Assignments of CclA*—To facilitate NMR studies, a {$^{15}N$,$^{13}C$}-labeled sample of CclA was prepared by growing the producer organism in isotopically enriched complex media. The $^{15}N$-HSQC spectrum of CclA shows good spectral dispersion, with 58 of the 60 amides displaying unique chemical shifts (supplemental Fig. 3). A suite of three-dimensional, triple resonance experiments allows full assignment of the backbone resonances of CclA (38). Chemical shift index analysis (39) of the $\alpha$-carbons suggests that CclA contains four distinct helices, separated by short loops (data not shown). In addition, chemical shift index values indicate that the N and C termini of CclA are involved in a helical segment. Complete side chain chemical shift assignments were achieved through a combination of homonuclear and heteronuclear multidimensional experiments.

*Structure of CclA*—The structure of CclA was calculated with CYANA 2.1 (30), using a combination of manually and automatically assigned distance constraints generated from NOE experiments and angle constraints from the HNHA experiment and the program TALOS (31). A family of 20 structures, representative of the solution structure of CclA, was obtained. This ensemble of structures is well superimposed, as shown in Fig. 1. The structural statistics for this ensemble of structures are listed in Table 1. CclA contains four helices, comprised of residues Gln$^{8}$–Ala$^{20}$ ($\alpha$1), Val$^{24}$–Leu$^{31}$ ($\alpha$2), Leu$^{38}$–Gln$^{52}$ ($\alpha$3), and Ile$^{54}$–Tyr$^{4}$ ($\alpha$4). The linkage between the N and C termini

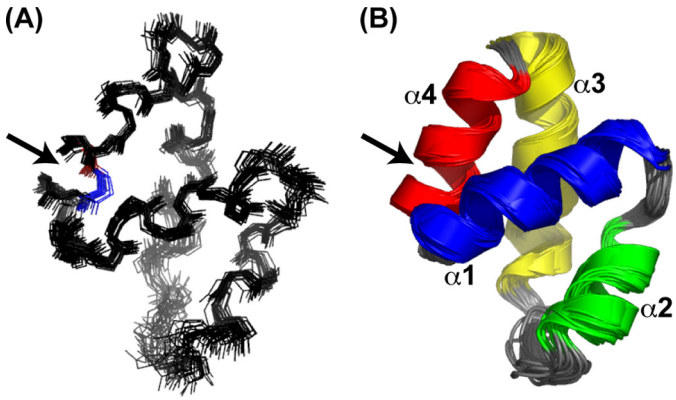


FIGURE 1. **Overlay of the 20 lowest energy conformers of CclA.** *A*, backbone representation. Residues 1 and 60, which are covalently linked by a peptide bond, are highlighted in *blue* and *red*, respectively. *B*, cartoon representation. Helices $\alpha$1, $\alpha$2, $\alpha$3, and $\alpha$4 are colored *blue*, *green*, *yellow*, and *red*, respectively. The N-to-C linkage is indicated with an *arrow*.

**TABLE 1**
**Structural statistics for CclA**[a]

| | |
|---|---|
| **NOE restraints** | 657 |
| Intraresidual ($\|i-j\|=1$) | 209 |
| Short range ($\|i-j\|\geq 1$) | 179 |
| Medium range ($1<\|i-j\|<5$) | 144 |
| Long range ($\|i-j\|\geq 5$) | 125 |
| **Dihedral angle restraints ($\Phi$ and $\Psi$)**[b] | 98 |
| **Coupling constants ($^{3}J_{HNH\alpha}$)** | 43 |
| **Ramachandran plot**[c] | |
| $\Phi/\Psi$ in most favored region | 94.0% |
| $\Phi/\Psi$ in additionally allowed region | 6.0% |
| $\Phi/\Psi$ in generously allowed region | 0.0% |
| $\Phi/\Psi$ in disallowed region | 0.0% |
| **Atomic r.m.s.d. (Å)** | |
| Backbone atoms (residues 1–60) | 0.62 ± 0.16 |
| Backbone atoms (residues 1–32 and 38–60) | 0.53 ± 0.12 |
| Heavy atoms (residues 1–60) | 1.02 ± 0.13 |
| Heavy atoms (residues 1–32 and 38–60) | 0.93 ± 0.09 |

[a] 20 lowest energy structures.
[b] Generated with TALOS.
[c] For residues 1–60.

of CclA is located within $\alpha$4. In general, the helices are connected by short, well defined loops. However, a longer, more flexible loop is located between helices 2 and 3. This region, spanning Gly$^{32}$ to Gly$^{37}$, contains three glycines and exhibits the highest degree of flexibility in the structure. When these six residues are excluded from the r.m.s.d. calculation, the r.m.s.d. of the ensemble decreases from 0.62 Å to 0.53 Å. The four helices of CclA are amphiphilic, with extensive packing of hydrophobic side chains into the interior of the protein (Fig. 2*A*). Several long range NOEs between hydrophobic side chains help stabilize the arrangement of the four helices.

*Surface Features of CclA*—Although most of the hydrophobic side chains of CclA are in the hydrophobic core, there are several solvent exposed hydrophobic residues (Fig. 2*B*). These residues form a hydrophobic strip that runs along the interface of $\alpha$1 and $\alpha$2. The crystal structure of AS-48 exhibits similar features, as the formation of a water soluble dimer arises from interactions between hydrophobic residues on the surfaces of $\alpha$1 and $\alpha$2 (21). As our results show that CclA does not form dimers in solution, these hydrophobic patches could assist interaction of the peptide with the lipophilic portion of the target membrane. CclA also has a hydrophobic cleft encircling

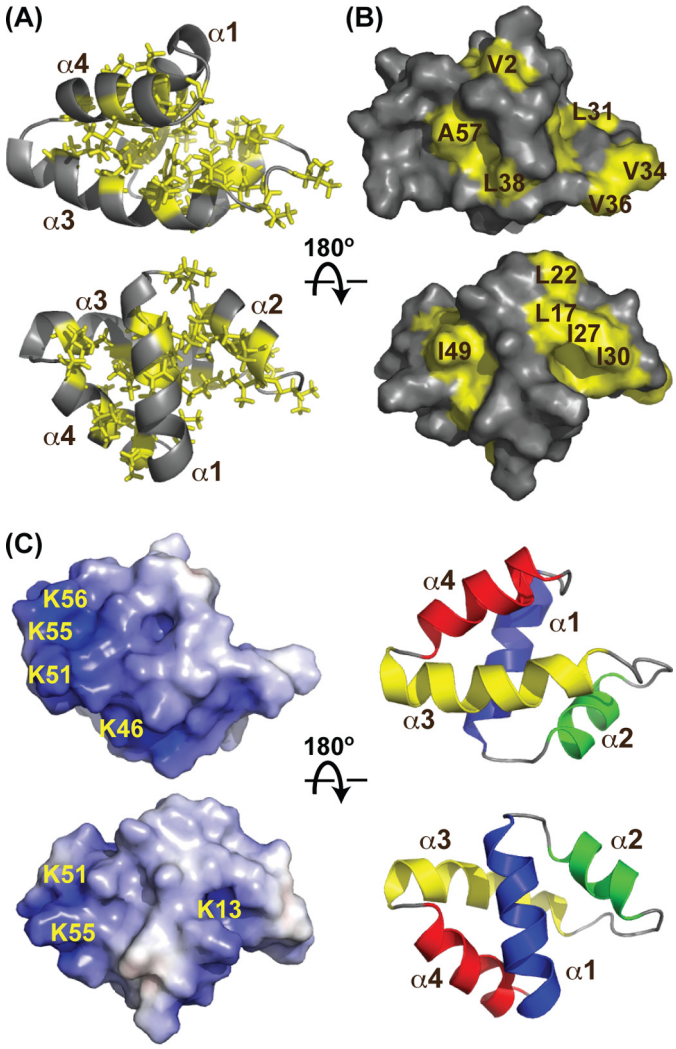


FIGURE 2. **Structural characteristics of CclA.** *A*, *ribbon diagram* depicting the compact, hydrophobic core of CclA. Hydrophobic sidechains are drawn as *sticks*. *B*, *surface plot* illustrating solvent exposed hydrophobic residues. *Yellow* indicates hydrophobicity from Ile, Leu, Val, and Phe. *C*, electrostatic surface potential of CclA. *Blue* and *red* indicate positive and negative charge, respectively. Key residues are labeled. The helical diagrams show the orientation of CclA.

the turns connecting α4/α1 and α2/α3. This region may be crucial for recognition and interaction with the enzyme(s) responsible for the cyclization of the N and C termini of CclA. The cyclization of CclA requires the loss of a four residue leader sequence (MLYE) and the covalent union of two leucine residues, ultimately located within α4. The point of linkage is surrounded by this cleft, and, as such, the hydrophobic nature of the cleft may facilitate interaction of the linear pre-CclA with the cyclization enzyme(s), help bring the termini of the peptide into close proximity, and stabilize the hydrophobic residues that must contact each other.

In addition to hydrophobic patches, the surface of CclA exhibits a prominent positive region, located along α3 and α4 (Fig. 2*C*). CclA contains five lysine residues, four of which are located within this stretch ($Lys^{46}$, $Lys^{51}$, $Lys^{55}$, and $Lys^{56}$). Again, a similar situation is seen with AS-48, wherein seven lysines reside in this section (20). In the case of AS-48, it has been suggested that this positive charge is essential for membrane insertion through a mechanism known as molecular electroporation (20, 23). According to this mechanism, when a peptide carrying sufficient charge density binds to the surface of a membrane, the local electric field associated with the peptide causes destabilization of the membrane, allowing for insertion of the peptide (40). However, it has also been shown that that this region alone is not sufficient for antibacterial activity. In 2004, Jiménez *et al.* (22) reported that a fragment of AS-48, bearing these charges and adopting a similar helical conformation to the native peptide, did not exhibit antibacterial activity. As such, this charged portion of the peptide must act in concert with other portions of the bacteriocin to exert the killing effect on target bacteria.

*Comparison of CclA to AS-48*—The structure of CclA is remarkably similar to that of AS-48, even though their sequences share only 30% identity. Both structures are highly compact, globular peptides, comprised of four or five helices enclosing a hydrophobic core. The two structures align surprisingly well, with an r.m.s.d. of ~3.0 Å across the entire sequence (Fig. 3). The superposition of CclA and AS-48 shows that in general, the helices are similar in length and assume similar orientations. For both structures, α1 and α2 are closely aligned, as are α4 of CclA and α5 of AS-48. In both molecules, the covalent linkage between the N and C termini resides in the last helix, at approximately the same three-dimensional location. In addition to having a similar architecture, CclA shares many surface features with AS-48, particularly the hydrophobic and cationic sections discussed above.

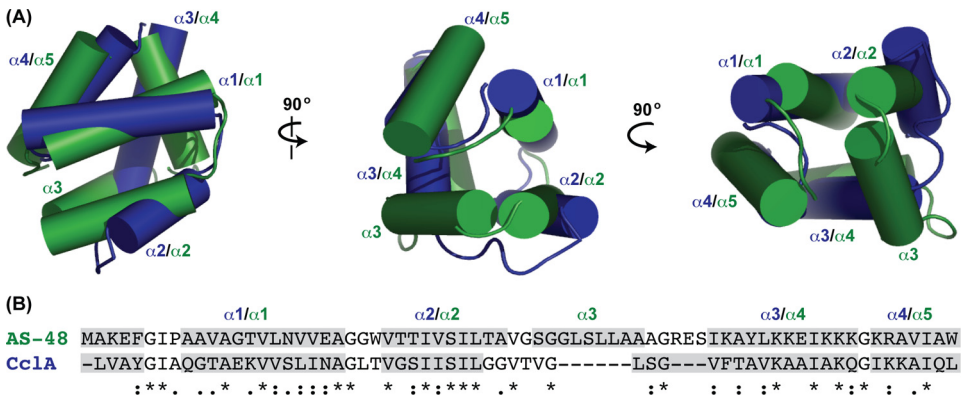


FIGURE 3. **Comparison of CclA and AS-48.** *A*, structural alignment of the two bacteriocins. CclA is *blue*, and AS-48 is *green*. The helices of each are labeled accordingly. *B*, sequence alignment of CclA and AS-48, according to ClustalW (36). Residues shaded in *gray* represent helical regions. Conserved residues are denoted with an *asterisk*; conservative substitutions are indicated with a *colon*, and semi-conservative substitutions are indicated with a *period*.

The most notable difference between CclA and AS-48 is that the latter contains an additional helix. Alignment of their structures illustrates that α3 of AS-48 and the extended strand of CclA occupy the same relative location. Because

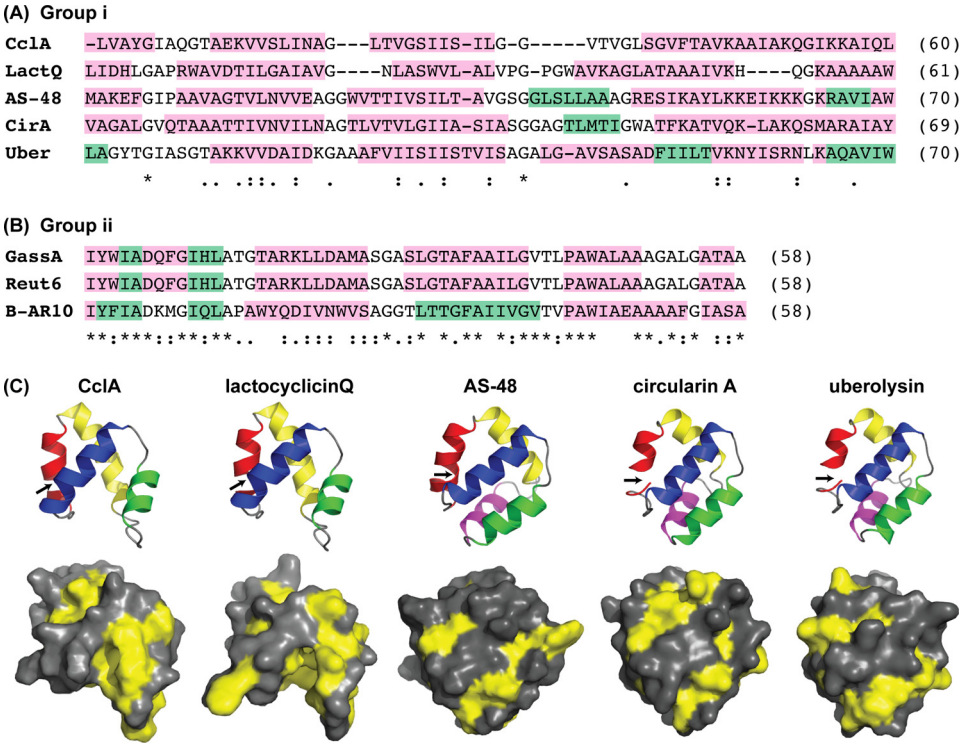


FIGURE 4. **Sequence alignment and predicted secondary structure for the group i and group ii circular bacteriocins.** Sequences were classified into groups i (*A*) and ii (*B*), as suggested by Cotter *et al.* (1) and aligned with ClustalW (36). Residues highlighted in *pink* are predicted to be helical, and residues highlighted in *green* are predicted to be either extended strand or helical. Conserved residues within are denoted with an *asterisk*; conservative substitutions are denoted with a colon, and semi-conservative substitutions are indicated with a *period*. *C*, structural features of the group i circular bacteriocins. Lactocyclicin Q was homology modeled after CclA, whereas circularin A and uberolysin were modeled after AS-48. The *top panel* depicts the helical orientation of the peptides, and the *bottom panel* illustrates hydrophobic patches resulting from L, I, V, M, F, and W (*yellow*). A *black arrow* indicates the position of the N-to-C cyclization.

Group i contains the disparate bacteriocins (CclA, lactocyclicin Q, AS-48, circularin A, and uberolysin), whereas the highly homologous bacteriocins (gassericin A, reutericin 6, and butyvibriocin AR10) comprise group ii. Our results reveal that even though CclA and AS-48 have low sequence identity, their three-dimensional structures are remarkably similar. Additionally, CD studies of gassericin A and reutericin 6 and sequence analysis of lactocyclicin Q indicate that these bacteriocins also contain helical secondary structure elements (11, 16). We propose that both groups of circular bacteriocins share the common overall structural motif of a saposin fold (25). To investigate this, we examined their potential structures through a combination of secondary structure prediction (using JPRED and PSI servers) and homology modeling (Fig. 4).

For the group i circular bacteriocins, sequence alignment shows that the greatest similarity exists among the N-terminal domain of these peptides, and this region is predicted to contain two distinct helices, ranging approximately from residues 8–20 and 20–34. For both CclA and lactocyclicin Q, a stretch of six or seven residues with a high number of helix breaking residues (glycines and prolines) is found after $\alpha$2, followed by a long helical section. Indeed, this prediction matches the observed structure of CclA in which a long extended loop separates $\alpha$2 from $\alpha$3 and a short tight loop demarks $\alpha$3/$\alpha$4. For the longer bacteriocins AS-48, circularin A, and uberolysin, an additional helical segment is predicted. As can been seen from the sequence alignment and the superposition of CclA with AS-48, this extra helix is located after $\alpha$2. Thus, it is likely that circularin A and uberolysin contain five helices (like AS-48), whereas the shorter circular bacteriocins have four helices. To further examine these structures, we performed homology modeling of the group i bacteriocins. Lactocyclicin Q was modeled after CclA, whereas circularin A and uberolysin were modeled after AS-48. For comparison, we also predicted the structure of CclA by threading it onto AS-48. The resulting model of CclA matched well to the experimental NMR solution structure, with very slight differences in the orientation of the four helices. The structural and surface features of CclA and AS-48 also match the predicted structures of the other bacteriocins of group i. All these bacteriocins have a nonpolar core with hydrophobic patches on their surfaces (Fig. 4*C*). In addition, they exhibit substantial positive patches on their surfaces, though in slightly different locations (supplemental Fig. 5). Inspection of the aligned pri-

CclA is shorter than AS-48 by 10 residues, it is unable to form a well defined helix at this site. Other differences can be observed between $\alpha$3 of CclA and $\alpha$4 of AS-48. In particular, $\alpha$3 of CclA is longer and has a slight bend, and its N-terminal portion does not overlay well with $\alpha$4 of AS-48. As can be seen from the overlay, the extended strand and kink in $\alpha$3 allows the shorter CclA to maintain its overall alignment with AS-48.

The program DALI (41) was used to identify proteins with similar features to CclA. As expected, the highest similarity was with AS-48 ($Z_{score}$ 6.9 and r.m.s.d. 2.7 Å across 58 residues). In addition, several saposin and saposin-like peptides were also identified. Saposins A and C (42), which act as lipid degrading enzymes and are known to interact with the cell membrane, were found to be remarkably similar to CclA (saposin A: $Z_{score}$ 4.5 and r.m.s.d. 2.4 Å across 53 residues; saposin C: $Z_{score}$ 3.9 and r.m.s.d. 2.4 Å across 50 residues), despite very low sequence similarity. In addition, the saposin-like peptides amoebapore A (43) and NK-lysin (25), which lyse bacterial and eukaryotic cells, also displayed high structural similarity to CclA (amoebapore A: $Z_{score}$ 4.2 and r.m.s.d. 2.9 Å across 54 residues; NK-lysin: $Z_{score}$ 3.2 and r.m.s.d. 2.6 Å across 51 residues). The sequence and structural alignment of CclA to these saposin and saposin-like peptides is illustrated in supplemental Fig. 4.

*Do the Circular Bacteriocins Share a Common Structural Motif?*—It has been suggested that the circular bacteriocins be divided into two subclasses according to their sequence (1).

mary sequences (Fig. 4*A*) shows that CclA, AS-48, and circularin A have a high density of basic residues toward the end of their C-terminal domains ($\alpha$3/$\alpha$a4 for CclA and $\alpha$4/$\alpha$5 for AS-48 and circularin A), whereas the sequence of uberolysin shows several basic residues in both the extreme N and C termini ($\alpha$5/$\alpha$1). Lactocyclicin Q differs from the other bacteriocins in this regard. Its basic residues are more uniformly distributed along the sequence of this peptide, with only a small positively charged patch located at the turn connecting $\alpha$3/$\alpha$4. The homology model of lactocyclicin Q also shows several negatively charged patches on the surface of this bacteriocin (supplemental Fig. 5).

For the highly homologous bacteriocins of subgroup ii (gassericin A, reutericin 6, and butyvibriocin AR10), sequence analysis predicts four helices, approximately equal in length, located between residues 16–25, 29–38, 40–49, and 52-5 (Fig. 4*B*). They are separated by short loops containing either glycines or prolines. This group, although homologous to each other, shares very low similarity to the group i bacteriocins. Furthermore, the physical properties of this subgroup are different, as these peptides contain many more acidic residues and have predicted isoelectric points (pI ~5) much lower that those of subgroup i (pI ~10). Nonetheless, it appears likely that the overall structure of this group of bacteriocins closely matches that of CclA, with four helices enclosing a compact hydrophobic core with an overall saposin fold.

*CclA Ion Channel Characteristics*—Recent studies have shown that CclA forms anion selective channels in lipid bilayers (27). We have further characterized the permeability of these channels by performing a series of anion substitution experiments, using either monatomic halide anions ($F^-$ and $Br^-$) or polyatomic monovalent anions ($H_2PO_4^-$, $NO_3^-$, and $CH_3COO^-$). For each anion, the observed single channel conductance was linear, within the range −100 mV to +100 mV (supplemental Fig. 6), and was equal to (in picosiemens): 50.2 ($F^-$), 163.4 ($Br^-$), 92.4 ($H_2PO_4^-$), 154.4 ($NO_3^-$), and 110.9 ($CH_3COO^-$). The permeability sequence, deduced from the reverse membrane potentials, follows the pattern $NO_3^- > Cl^- > CH_3COO^- > F^- > Br^- > H_2PO_4^-$ and corresponds to the sixth Eisenman permeability sequence (44). This pattern suggests that the electrostatic interaction energy between an anion and a channel binding site is much larger than the dehydration energy needed to tear the permeant anion out of water (44).

We also examined the effect of pH on the functional properties of the CclA pores. Under different pH conditions, the *I–V* relationship for the CclA channels were linear and acidic conditions facilitated channel conductance (supplemental Fig. 7). Under symmetric conditions, the conductance was measured to be 134.8, 154.1, and 226.8 picosiemens at pH 9.0, 7.4, and 5.5, respectively. The largest conductance (372.2 picosiemens) was observed under asymmetric conditions in which the *cis* chamber was set at pH 5.5, and the *trans* chamber was set at pH 7.4. These results suggest that the pH of the solution does not affect channel conformation, as conductance was observed at all of the pH values tested. This is in agreement with our NMR studies that show minimal change in spectral dispersion of CclA across a broad range of pH conditions.

Although pH does not affect channel conformation, it has a pronounced effect on the stability of the CclA pore. Under acidic conditions, greater conductance is observed, suggesting that the CclA ion channel is more stable and that anion permeation is facilitated. At neutral pH, the five lysine side chains of CclA would be protonated, imparting a localized, positive charge on the molecule. At lower pH, the side chain of $Glu^{12}$ would also be protonated, further enhancing the net positive charge of the molecule. This net positive charge is likely a key component in both attracting CclA to the anionic lipid membrane and facilitating membrane insertion via molecular electroporation (40). A similar argument has been proposed in the case of pore formation by AS-48 (20, 23).

Unlike AS-48, pore formation by CclA is voltage-dependant; the membrane potential affects both CclA channel activation and kinetics. Channel activation occurs with negative potential (−100 mV) and subsequent inactivation with positive potential (100 mV) (supplemental Fig. 8*A*). This effect occurs on the time scale of seconds to minutes, and thus, is much slower than the voltage-dependent effects observed in voltage-gated ion channels, such as sodium and potassium channels (45). CclA channel gating is affected by applied membrane potentials (supplemental Fig. 8*B*). At −100 mV, the averaged open time was 1.6 s and 3.1 s at −80 mV. The membrane potential had no significant effect on CclA channel gating in the range of −40 to 40 mV (data not shown).

*Fluoride Binding to CclA*—Because our functional studies revealed that CclA is capable of transporting fluoride ions, we examined the interaction between fluoride and CclA by NMR. In an initial set of experiments, CclA was titrated with sodium fluoride, and the chemical shift of the fluoride was monitored by $^{19}F$ NMR. The results reveal at least two modes of binding between fluoride and CclA (Fig. 5). Prior to the addition of exogenous fluoride, a small peak at −156.9 ppm is apparent. This endogenous fluoride likely originates from exposure to Teflon®, which has been shown to produce small amounts of fluoride ion in aqueous solution (46). Excess CclA immediately captures this. Upon addition of sodium fluoride (0.5 and 1.0 molar eq), another peak appears at −156.3 ppm. Further addition of sodium fluoride (1.5, 2.0, and 3.0 molar eq) yields a third peak at −155.2 ppm. This third peak has a chemical shift equivalent to that observed for fluoride anion in the absence of CclA (pH 3.8) and represents unbound fluoride. Thus, the results indicate at least two different binding modes between CclA and fluoride. At low concentrations of anion, fluoride assumes one particular mode of binding; this mode is subsequently replaced by another as the concentration of this anion increases and exceeds a molar equivalent.

Because the interaction between fluoride and CclA could be observed by $^{19}F$ NMR, the effect of fluoride on the backbone amides and lysine side chains of CclA was examined by NMR spectroscopy. Upon addition of sodium fluoride, no changes in the backbone amides of CclA were observed in the regular $^{15}N$-HSQC spectrum. Using an upfield $^{15}N$-HSQC experiment, three of the five lysine $\epsilon$-amino groups were detected, and the identity of these groups was assigned with a $^{15}N$-TOCSY-HSQC spectrum (details are listed in the supplemental data). However, no significant changes in the spectra of these side

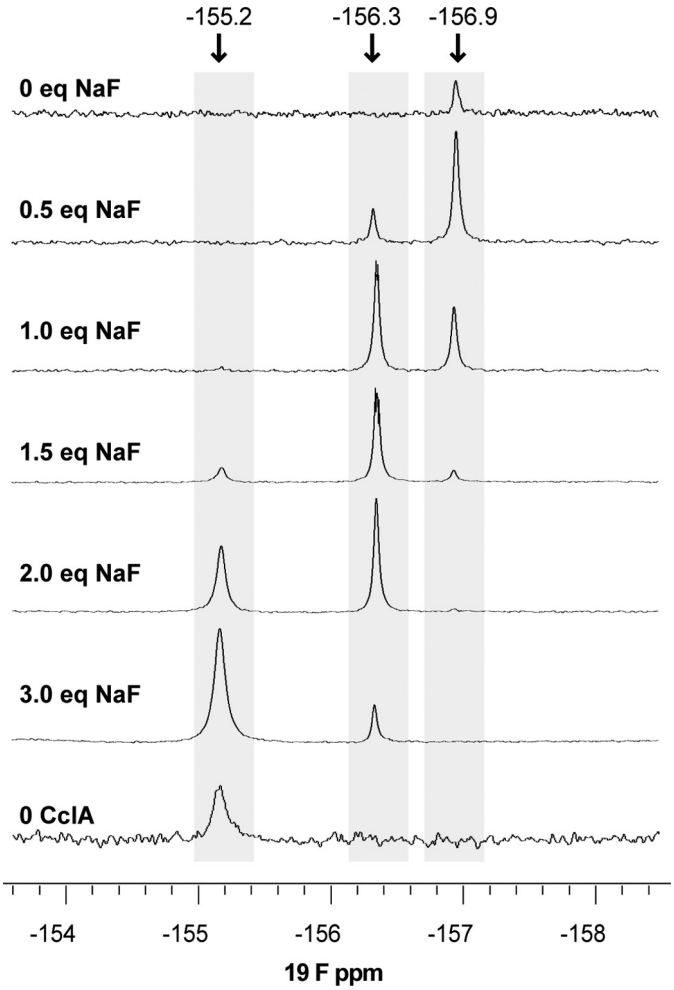


FIGURE 5. **$^{19}$F NMR spectra of sodium fluoride titrated against CclA (1 mM in 90% $H_2O$ and 10% $D_2O$, pH 3.8).** Spectra were recorded on a 500 MHz Varian VNMRS spectrometer. The fluoride signal present in the 0 eq sodium fluoride spectrum is due to endogenous fluoride interacting with CclA.

chains were detected when fluoride was added. This is not surprising, as CclA binds and transports different anions, including acetate and presumably trifluoroacetate. Purified CclA contains trifluoroacetate as its counterion from the HPLC purification, which can be seen by a large peak at −78 ppm in the $^{19}$F NMR spectrum. Hence, prior to addition of sodium fluoride, the residues involved in fluoride binding are likely already held in an anion-binding conformation due to interaction with trifluoroacetate, and no significant structural rearrangement of CclA occurs. Similarly, the effect of other anions (phosphate and chloride) on the backbone structure of CclA did not result in any detectable changes by $^{15}$N-HSQC. Taken together, the results suggest that the two different peaks observed by $^{19}$F NMR for fluoride bound to CclA may be due to different hydrogen-bonding ligands (*e.g.* water and protonated $\epsilon$-amino groups of lysine) attached to this anion at a single site.

In summary, our studies show that despite varied sequence similarity, the circular bacteriocins likely share a common structural motif. This consists of four or five conserved $\alpha$ helices enclosing a compact hydrophobic core with the common architecture of the saposin fold. The bacteriocins with longer primary sequences are able to adopt the additional helix, which is located after helix $\alpha$2. This architecture imparts unique stability to these potent antimicrobial peptides and undoubtedly mediates their individual modes of action at the target membrane. The structures of CclA and AS-48 and the homology models of circularin A, uberolysin, and lactocyclicin Q show that a cluster of basic residues imparts a highly localized positive charge on the surface of the peptide. This conserved motif is likely responsible for attracting the peptides to the surface of the anionic target membrane. Differences in individual mechanism, such as anion transport by CclA and pore creation by AS-48, most likely result from variations of surface features on the conserved framework. Further structural and mutational studies on the circular bacteriocins will help elucidate how these peptides exert their killing action.

*Acknowledgments—We thank Tara Sprules (Biochemistry, McGill University), Ryan McKay (National High School Nuclear Magnetic Resonance Centre, University of Alberta), and Mark Miskolzie for assistance in acquiring NMR spectra and to Kamaljit Kaur (Department of Pharmacy, University of Alberta) for discussions regarding homology modeling. We thank Olivier Julien and Pascal Mercier for assistance with CYANA and Maia Cherney and Sheraz Khan (Department of Biochemistry, University of Alberta) for help with dynamic light scattering measurements.*

## REFERENCES

1. Cotter, P. D., Hill, C., and Ross, R. P. (2005) *Nat. Rev. Microbiol.* **3,** 777–788
2. Nes, I. F., Yoon, S. S., and Diep, W. B. (2007) *Food Sci. Biotechnol.* **16,** 675–690
3. van Belkum, M. J., and Stiles, M. E. (2000) *Nat. Prod. Rep.* **17,** 323–335
4. Maqueda, M., Sánchez-Hidalgo, M., Fernández, M., Montalbán-López, M., Valdivia, E., and Martínez-Bueno, M. (2008) *FEMS Microbiol. Rev.* **32,** 2–22
5. Craik, D. J. (2006) *Science* **311,** 1563–1564
6. Craik, D. J., Daly, N. L., Saska, I., Trabi, M., and Rosengren, K. J. (2003) *J. Bacteriol.* **185,** 4011–4021
7. Martin-Visscher, L. A., van Belkum, M. J., Garneau-Tsodikova, S., Whittal, R. M., Zheng, J., McMullen, L. M., and Vederas, J. C. (2008) *Appl. Environ. Microbiol.* **74,** 4756–4763
8. Samyn, B., Martinez-Bueno, M., Devreese, B., Maqueda, M., Gálvez, A., Valdivia, E., Coyette, J., and Van Beeumen, J. (1994) *FEBS Lett.* **352,** 87–90
9. Kalmokoff, M. L., Cyr, T. D., Hefford, M. A., Whitford, M. F., and Teather, R. M. (2003) *Can. J. Microbiol.* **49,** 763–773
10. Kemperman, R., Kuipers, A., Karsens, H., Nauta, A., Kuipers, O., and Kok, J. (2003) *Appl. Environ. Microbiol.* **69,** 1589–1597
11. Kawai, Y., Ishii, Y., Arakawa, K., Uemura, K., Saitoh, B., Nishimura, J., Kitazawa, H., Yamazaki, Y., Tateno, Y., Itoh, T., and Saito, T. (2004) *Appl. Environ. Microbiol.* **70,** 2906–2911
12. Kawai, Y., Saito, T., Kitazawa, H., and Itoh, T. (1998) *Biosci. Biotechnol. Biochem.* **62,** 2438–2440
13. Kawulka, K., Sprules, T., McKay, R. T., Mercier, P., Diaper, C. M., Zuber, P., and Vederas, J. C. (2003) *J. Am. Chem. Soc.* **125,** 4726–4727
14. Babasaki, K., Takao, T., Shimonishi, Y., and Kurahashi, K. (1985) *J. Biochem.* **98,** 585–603
15. Wirawan, R. E., Swanson, K. M., Kleffmann, T., Jack, R. W., and Tagg, J. R. (2007) *Microbiology* **153,** 1619–1630
16. Sawa, N., Zendo, T., Kiyofuji, J., Fujita, K., Himeno, K., Nakayama, J., and Sonomoto, K. (2009) *Appl. Envir. Microbiol.* **75,** 1552–1558
17. Leer, R. J., van der Vossen, J. M. B. M., van Giezen, M., van Noort, J. M., and Pouwels, P. H. (1995) *Microbiology* **141,** 1629–1635
18. Kawulka, K. E., Sprules, T., Diaper, C. M., Whittal, R. M., McKay, R. T., Mercier, P., Zuber, P., and Vederas, J. C. (2004) *Biochemistry* **43,** 3385–3395

19. Zheng, G., Yan, L. Z., Vederas, J. C., and Zuber, P. (1999) *J. Bacteriol.* **181,** 7346–7355
20. González, C., Langdon, G. M., Bruix, M., Gálvez, A., Valdivia, E., Maqueda, M., and Rico, M. (2000) *Proc. Natl. Acad. Sci. U.S.A.* **97,** 11221–11226
21. Sánchez-Barrena, M. J., Martínez-Ripoll, M., Gálvez, A., Valdivia, E., Maqueda, M., Cruz, V., and Albert, A. (2003) *J. Mol. Biol.* **334,** 541–549
22. Jiménez, M. A., Barrachi-Saccilotto, A. C., Valdivia, E., Maqueda, M., and Rico, M. (2005) *J. Pept. Sci.* **11,** 29–36
23. Maqueda, M., Gálvez, A., Bueno, M. M., Sanchez-Barrena, M. J., González, C., Albert, A., Rico, M., and Valdivia, E. (2004) *Curr. Protein Pept. Sci.* **5,** 399–416
24. Gálvez, A., Maqueda, M., Martínez-Bueno, M., and Valdivia, E. (1991) *J. Bacteriol.* **173,** 886–892
25. Liepinsh, E., Andersson, M., Ruysschaert, J. M., and Otting, G. (1997) *Nat. Struct. Biol.* **4,** 793–795
26. John, M., Wendeler, M., Heller, M., Sandhoff, K., and Kessler, H. (2006) *Biochemistry* **45,** 5206–5216
27. Gong, X., Martin-Visscher, L. A., Nahirney, D., Vederas, J. C., and Duszyk, M. (2009) *Biochim. Biophys. Acta* (*Biomembranes*) **1788,** 1797–1803
28. Delaglio, F., Grzesiek, S., Vuister, G. W., Zhu, G., Pfeifer, J., and Bax, A. (1995) *J. Biomol. NMR* **6,** 277–293
29. Johnson, B. A., and Blevins, R. A. (1994) *J. Biomol. NMR* **4,** 603–614
30. Güntert, P., Mumenthaler, C., and Wüthrich, K. (1997) *J. Mol. Biol.* **273,** 283–298
31. Cornilescu, G., Delaglio, F., and Bax, A. (1999) *J. Biomol. NMR* **13,** 289–302
32. Baker, N. A., Sept, D., Joseph, S., Holst, M. J., and McCammon, J. A. (2001) *Proc. Natl. Acad. Sci. U.S.A.* **98,** 10037–10041
33. Cole, C., Barber, J. D., and Barton, G. J. (2008) *Nucleic Acids Res.* **36,** W197–W201
34. McGuffin, L. J., Bryson, K., and Jones, D. T. (2000) *Bioinformatics* **16,** 404–405
35. Jones, D. T. (1999) *J. Mol. Biol.* **292,** 195–202
36. Larkin, M. A., Blackshields, G., Brown, N. P., Chenna, R., McGettigan, P. A., McWilliam, H., Valentin, F., Wallace, I. M., Wilm, A., Lopez, R., Thompson, J. D., Gibson, T. J., and Higgins, D. G. (2007) *Bioinformatics* **23,** 2947–2948
37. Guex, N., and Peitsch, M. C. (1997) *Electrophoresis* **18,** 2714–2723
38. Zerbe, O. (2003) *BioNMR in Drug Research* (Zerbe, O., ed) pp. 79–92, Wiley-VCH, Weinheim
39. Wishart, D. S., and Sykes, B. D. (1994) *J. Biomol. NMR* **4,** 171–180
40. Miteva, M., Andersson, M., Karshikoff, A., and Otting, G. (1999) *FEBS Lett.* **462,** 155–158
41. Holm, L., Kääriäinen, S., Rosenström, P., and Schenkel, A. (2008) *Bioinformatics* **24,** 2780–2781
42. Ahn, V. E., Leyko, P., Alattia, J. R., Chen, L., and Privé, G. G. (2006) *Protein Sci.* **15,** 1849–1857
43. Hecht, O., van Nuland, N. A., Schleinkofer, K., Dingley, A. J., Bruhn, H., Leippe, M., and Grotzinger, J. (2004) *J. Biol. Chem.* **279,** 17834–17841
44. Wright, E. M., and Diamond, J. M. (1977) *Physiol. Rev.* **57,** 109–156
45. Hille, B. (1992) *Ionic Channels of Excitable Membranes*, 2nd Ed., Sinauer Associates, Sunderland, MA
46. Lai, C.-Z., Koseoglu, S. S., Lugert, E. C., Boswell, P. G., Rbai, J., Lodge, T. P., and Bhlmann, P. (2009) *J. Am. Chem. Soc.* **131,** 1598–1606